Dynamic Initiation Fracture Toughness Determination and Full-field Strain Measurements of Rock Material

Qianbing ZHANG [a], Wei WU [b]

École Polytechnique Fédérale de Lausanne, School of Architecture, Civil and Environmental Engineering, Laboratory of Rock Mechanics, CH-1015 Lausanne, Switzerland

[a] qianbing.zhang@epfl.ch, [b] wei.wu@epfl.ch

Keywords: Dynamic initiation fracture toughness; full-field strain field; rock material; digital image correlation; split Hopkinson pressure bar.

Abstract. The purpose of this paper is to present a detailed experimental procedure for the quantitative determination of initiation fracture toughness and full-field strain measurement of rock material under dynamic loads. Notched semi-circular bending tests were conducted using a split Hopkinson pressure bar (SPHB) system. Experimental setup, data acquisition and interpretation were described in detail. The digital image correlation (DIC) technique combining with a high-speed cameral was adopted for the measurement of surface deformation characteristics of rock specimens. To verify the accuracy of this technique, comparative tests were performed in which the strains in the specimens were simultaneously determined using the DIC technique and on-specimen strain gauges. Strain gauges were also used to determine the time-to-fracture. Experimental results show that (1) dynamic crack initiation toughness can be well determined; and (2) the high-speed DIC technique provides reliable full-field strain fields in the specimens under dynamic loads.

Introduction

Dynamic loads are usually associated with high amplitude and short duration stress pulse. Information regarding mechanical properties of rock material is of considerable importance in assessing the stability of rock structures under dynamic loads. A substantial effort has been made towards investigating the mechanical behaviour of rock materials over a wide range of loading rates (e.g., [1-5]). Unfortunately, no standard has yet been set for determining dynamic mechanical properties of rock materials. Although one has recently been suggested [6], there are still some problems that remain to be resolved. Some novel work still need to be conducted in order to bring some further insights into this issue, and thus enabling information on dynamic mechanical behavior of rock materials is to be reliably and easily obtained.

Full-field optical measurement techniques are very promising tools to analyze mechanical properties and measure deformation of materials and structures [7]. The digital image correlation (DIC) technique is such a method, originally proposed by [8], which has become a popular method for measuring surface deformation across a wide range of length and time scales. On the one hand, the technique has no inherent length scale, and thus is applicable to experiments covering a broad range of fields of view not only from nano-/micro-scale to field-scale, but also from two-dimensional (2D) to three-dimensional (3D). On the other hand, to be satisfied with the recent progress in the advent of high-speed cameras with high-spatial and temporal resolutions, advanced image processing methods and high speed computations, the DIC technique has also been applied testing over a wide range of loading rates.

In the present study, the notched semi-circular bending (SCB) method was conducted using a split Hopkinson pressure bar (SPHB) system. Experimental setup, data acquisition and interpretation were described in detail. The DIC technique combining with high-speed cameral was adopted to

directly measure full-field strain fields. Strain gauges were also used to determine the time-to-fracture, and the results were compared and validated with computed results by the DIC technique.

Experimental Setup

Rock Material. The rock material used in the study was a fine-grained marble widely available in the Fangshan area of Beijing, China. Microscopic studies were performed to give an insight of the mineralogical composition and grain sizes. The Fangshan marble consists of dolomite (~98%) and quartz (~2%) and the size of minerals is from 10 to 200 μm with the average dolomite size of 100 μm and the average quartz size of 200 μm. The physical and mechanical properties tested according to standard methods were summarized in Table 1.

Table 1 Summary of physical and mechanical properties of the Fangshan marble (average value)

ρ_s [kg/m^3)]	σ_c [Mpa]	σ_t [Mpa]	K_{IC} [MPa m$^{1/2}$]	E_s [Gpa]	ν	C_s [m/s]
2800	155	9.5	3.0	85	0.28	6000

Note: ρ_s-Density; σ_c-Uniaxial compressive strength; σ_t-Tensile strength; K_{IC}-Mode I fracture toughness; E_s-Young's modulus; ν-Poisson's ratio; C_s-Dilatational wave speed of the specimen.

The Split Hopkinson Pressure Bar System. In the present study, dynamic tests were conducted using the SHPB with the cone-shaped striker [9]. A schematic of experimental setup is shown in Fig. 1 and it consists of

- Gas gun, a cone-shaped striker (0.5 m), incident bar (2 m), transmission bar (1.5 m), momentum bar (0.5 m) and momentum trap,
- a laser-beam velocity measurement system,
- two pairs of strain gauges glued on bars connecting to Wheatstone bridge,
- a CS-1D super dynamic strain meter (8 channels, 1-MHz A/D converter),
- a DL750 ScopeCorder digital oscilloscope (Yokogawa®),
- a high-speed imaging system
- a computer with integrated data acquisition and image processing software.

Data Acquisition and Validation of SHPB. Favorable locations for the strain gauges are ideally such that the incident and reflected waves do not overlap as shown in Fig. 2. Strain gauge signals are recorded using a high speed digital oscilloscope with a higher sampling rate (10 MS/s) and a 12-bit isolation module and preferably with differential inputs to reduce noise. The threshold of electric potential of Transistor-Transistor-Logic (TTL) pulse generated by strain gauge on the incident bar should be preset to trigger the oscilloscope. All of the raw data just as observed on the oscilloscope are processed as described after being digitally filtered with a low-pass filter with a cutoff frequency of 10,000 Hz. This is done to remove the very high frequency bit noise that overlays the strain signals and resulted in robust algorithms for detecting the time-of-arrival of the stress wave.

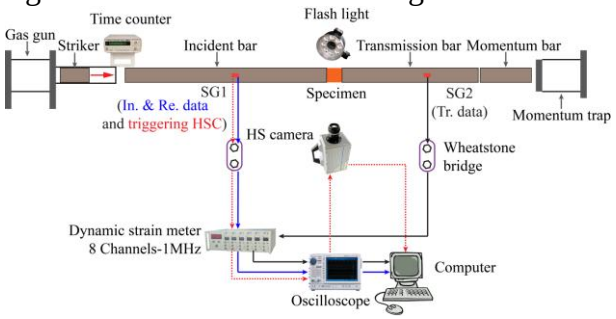

Fig. 1 Schematic of the SHPB system

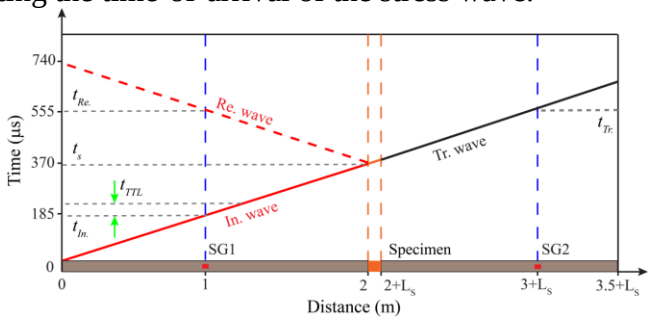

Fig. 2 Lagrangian wave propagation diagram

Dynamic Testing Method. The SCB testing method, originally proposed by Chong [10] for determining Mode I fracture toughness, has been used worldwide. The schematic of SCB specimen is shown in Fig. 3(a). The equation for the quasi-static stress intensity factor (SIF) is expressed as,

$$K_I = Y_I(\frac{S}{R})\frac{P\sqrt{\pi a}}{DB} \quad (1)$$

where K_I is the quasi-static SIF, $Y_I(S/R)$ is Mode I geometry factor, $2S$ is the span of the SCB specimen, R is the specimen radius, P is applied force on the specimens, a is the crack length, D is the specimens diameter, B is the specimens thickness. For $S/R = 0.67$ and $a/R = 0.2$, $Y_I(S/R)$ can be derived as [11],

$$Y_I(\frac{S}{R}) = 3.638 - 0.139(\frac{a}{R}) + 0.039\exp(7.387(\frac{a}{R})) \quad (2)$$

In dynamic tests, the time dependent load $P(t)$ replaces the quasi-static value in Eq. (1) resulting in the SIF being a function of time called dynamic SIF (K_I^{dyn}).

$$K_I^{dyn} = Y_I(\frac{S}{R})\frac{P(t)\sqrt{\pi a}}{DB} \quad (3)$$

The dynamic crack initiation toughness (K_{Id}) is then found by evaluating Eq. (3) at the time-to-fracture (t_f), as shown in Eq. (4),

$$K_{Id}(\dot{K}_I^{dyn}) = K_I^{dyn}(t_f) = Y_I(\frac{S}{R})\frac{P(t_f)\sqrt{\pi a}}{DB} \quad (4)$$

The loading rate ($\dot{K}_I^{dyn}$), expressed in terms of dynamic SIF rate, is calculated by the average K_{Id} and the average t_f. The calculation gives a reasonable value of the loading rates without fitting dynamic SIF curve because the rise time of the applied load is near linear.

Two strain gauges were glued in accordance with the tensile direction and aligned along the loading diameter. SG1 with a distance (d_1) of 2 mm from the crack tip was used to determine the time-to-fracture (t_f), and SG2 glued with a distance of 10 mm from SG1 was applied to measure the propagating crack speed v.

High-speed Camera Settings and Synchronization. The high speed imaging system consists of a Complementary Metal-Oxide Semiconductor (CMOS) sensor-based high-speed camera (Photron Fastcam SA1.1), a macro-lens (Kenko PRO 300 2.0× objective lens), a set of extension tube (Kenko 12, 20 and 36 mm), and a ring-shaped flash light (Pallite VIII 120V).

The high-speed camera was located at a safety distance of 0.5 m from the specimen in order to avoid damage and camera motion induced by the blasting pieces. Thus, a macro-lens was necessary for getting the close view of specimens. The best way to check the camera motion was setting a number of stationary points in the background, which could be used to correct cameral calibration for each

image. Random speckle pattern of spray paint was applied to mark the specimen surface and to ensure good contrast of the images, as shown in Fig. 3(b).

(a) Schematic diagram (b) Photographic view

Fig. 3 Setup of semi-circular bending (SCB) specimen (ZOC-Zone of camera, ZOI-Zone of interest for computing of DIC; specimen dimensions are R=25 mm, 2S = 33.3 mm, B = 20 mm, a = 5 mm)

In this study, the camera was operated at setting: 256 by 144 array size, 8 μs inter-frame time [125, 000 frame per second (fps)]. High-speed camera was triggered by a TTL pulse and synchronized within 100 ns time delay using 2 m network cable connecting to a high speed oscilloscope. Therefore the time of capturing HS-images started from the time triggered by the TTL pulse, and the number of captured images could be obtained until the stress wave arrived at the specimen,

$$n = \frac{t_s - t_{In.} - t_{TTL}}{t_{frame}} \tag{5}$$

where t_s is the time-of-arrival of the specimen, $t_{In.}$ is the time-of-arrival of the incident wave, t_{TTL} is the time triggered by a TTL pulse that is determined from the incident wave data, as clearly indicated and shown in Fig. 2, t_{frame} is the inter-frame time of high-speed camera.

Principle of Digital Image Correlation

The basic principle of DIC is the matching of the same pixels between two images recorded before and after deformation, as shown in Fig. 4. In order to compute the displacements of point P, a square reference subset of $(2M+1)\times(2M+1)$ pixels centered at point $P(x,y)$ from the reference image is chosen and used to track its corresponding location in the deformed image. The DIC algorithms aim to find the displacements, ***u*** and ***v***, of the center of each pixel subset. If the center of a subset displaces an amount indicated by ***u*** and ***v***, then the coordinates in the initial image (x_i, y_i), of any pixel in that subset are related to their displaced coordinates in the deformed image (x_i', y_i'), by:

$$x_i' = x_i + u + \frac{\partial u}{\partial x}\Delta x + \frac{\partial u}{\partial y}\Delta y,\ y_i' = y_i + v + \frac{\partial v}{\partial x}\Delta x + \frac{\partial v}{\partial y}\Delta y \tag{6}$$

where Δx and Δy are distances from the subset center to point (x_i, y_i). Partial derivatives of the displacements are included to account for small straining of the subset. The correspondence of pixel intensity values between two subsets, then, is measured using the zero-normalized cross-correlation (ZNCC), which can be written in form as Eq. (7) [8],

$$C_{ZNCC}=\frac{\sum_{i=-M}^{M}\sum_{j=-M}^{M}[f(x_i,y_j)-f_m]\times[g(x_i^{'},y_j^{'})-g_m]}{\sqrt{\sum_{i=-M}^{M}\sum_{j=-M}^{M}[f(x_i,y_j)-f_m]^2}\sqrt{\sum_{i=-M}^{M}\sum_{j=-M}^{M}[g(x_i^{'},y_j^{'})-g_m]^2}} \tag{7}$$

where, $f(x_i,y_i)$ is the gray level intensity at coordinates (x_i,y_i) in the reference subset of the reference image and $g(x_i^{'},y_j^{'})$ is the gray level intensity at coordinates $(x_i^{'},y_j^{'})$ in the target subsets of the deformed images; $f_m=1/(2M+1)^2\sum_{i=-M}^{M}\sum_{j=-M}^{M}f(x_i,y_j)$ and $g_m=1/(2M+1)^2\sum_{i=-M}^{M}\sum_{j=-M}^{M}g(x_i^{'},y_j^{'})$ are the mean intensity values of reference and target subsets, respectively. The DIC technique described above is implemented in Matlab (MathWorks®) to estimate in-plane surface strain fields [12].

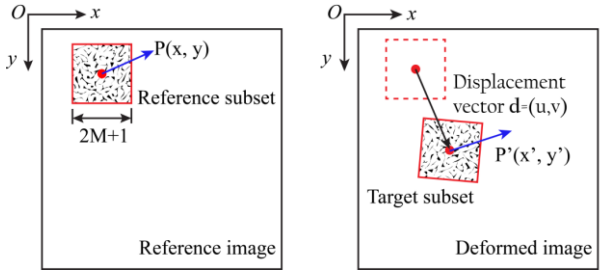

Fig. 4 Schematic of a reference subset before deformation and a target subset after deformation

Experimental Data Interpretation and Discussion

The combining methods of strain gauge and the high-speed DIC were adopted to detect the time-to-fracture, and the dynamic fracture toughness was determined by the quasi-static theory when the requirement of stress equilibrium in the specimen was satisfied.

Fig. 5(a) represented a typical testing result with a striking velocity of 2.25 m/s. Ten images were captured before the stress wave arrived at the specimen calculated using Eq. (5) and the value indicated in Fig. 5(b). It can be seen from Fig 5(c) that the time-to-fracture of SG1 (t_{1f}) was about 40 μs and the time of crack propagating from SG1 to SG2 (t_{12}) was approximately 15 μs. Therefore, the time-to-fracture of the specimen was determined by Eq. (8),

$$t_f=t_{1f}-t_1 \tag{8}$$

where d_1 is the distance between the crack tip and the position of SG1 (2 mm), t_1 is the time of crack propagating from the crack tip to SG1 ($t_1=d_1/v_1$. Since the crack speed v_1 is hard to exactly determine using strain gauges or high-speed camera, in the study, the crack speed v_{12} was used to estimate. $v_{12}=d_{12}/t_{12}\approx 667m/s$, where d_{12} is the distance between SG1 and SG2). Therefore, the time-to-fracture was approximately 37 μs. The reason why the crack speed v_{12} used would also be explained in the following part.

It was shown in Fig. 5(d) that the specimen was in a state of stress equilibrium through the time-to-fracture. It can been seen from Fig. 5(e), individual white belt developed from the pre-notched tips

in response to loading prior to the initiation of any macroscopic observable crack, as indicated by a dashed arrow. The crack initiated at about 38 μs, after initiation, the observable crack tip formed and the crack tip position was denoted as a solid arrow.

The first image (0 μs) was chosen as the reference image and a size of zone-of-interest (ZOI) of 150 by 95 pixels was selected for correlation calculation. The size of one pixel was equivalent to 0.11 mm in the specimen. The vertical strain fields were shown in Fig. 5(f). It can be noted that the maximum contours of strain field were concentrated around the tip of pre-notched crack, and it can also be seen that the localized strain was propagating and evolving along the pre-notch direction with applied load increasing.

From the HS-images, crack speed was calculated according to the crack tip position and the corresponding time. Once initiated, the crack accelerated along the pre-notched crack direction reaching speeds up to 680 m/s, which was approximately 25% of the shear wave speed of the Fangshan marble (2800 m/s). The crack speeds from some experiments were also calculated and plotted as a function of time in Fig. 5(g). The speeds all showed the same acceleration across the specimen with an initial increase and then leveling off. It was observed that typically some radially angled cracks formed at loading point of the specimen closing to the incident bar side that was subjected to a higher strain rate. The dynamic crack initiation toughness was approximately $3.3\,GPa\sqrt{m}$ at the loading rate of $90\,GPa\sqrt{m}/s$, as shown in Fig. 5(h). However, all SIF data to the right of the vertical becomes a function of the moving crack's speed. This process is typically identified as dynamic crack growth toughness that is outside the scope of this research.

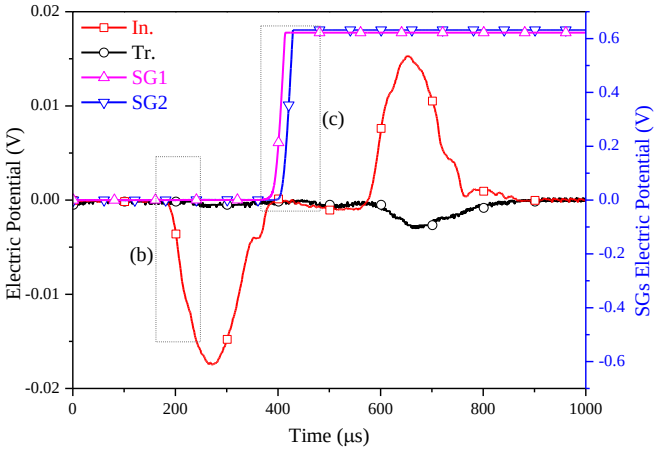

(a) Raw data of a typical SCB test

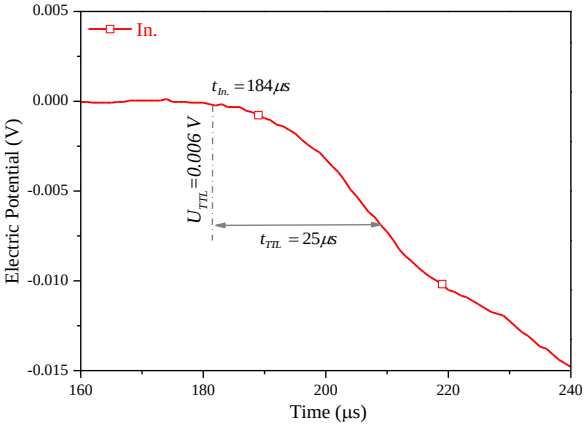

(b) Magnitude of the partial incident wave

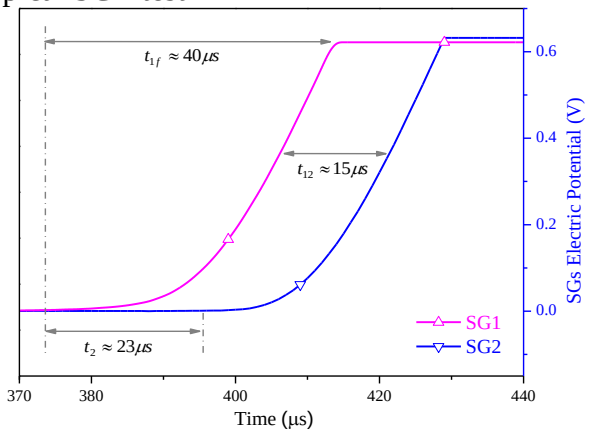

(c) Magnitude of the partial data of strain gauges

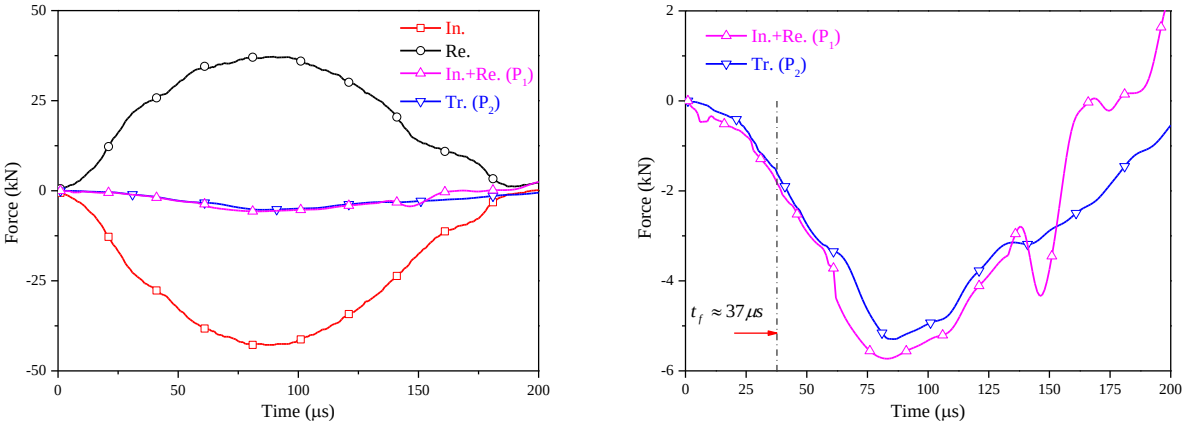

(d) Dynamic force equilibrium check

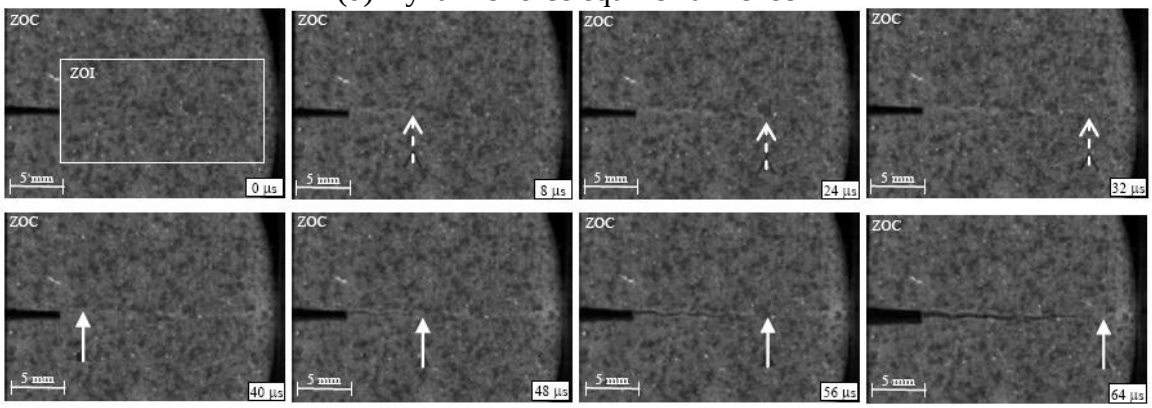

(e) HS-images at different stages

(The development of white belt indicated by a dashed arrow, and the observable crack-tip is indicated by a solid arrow.)

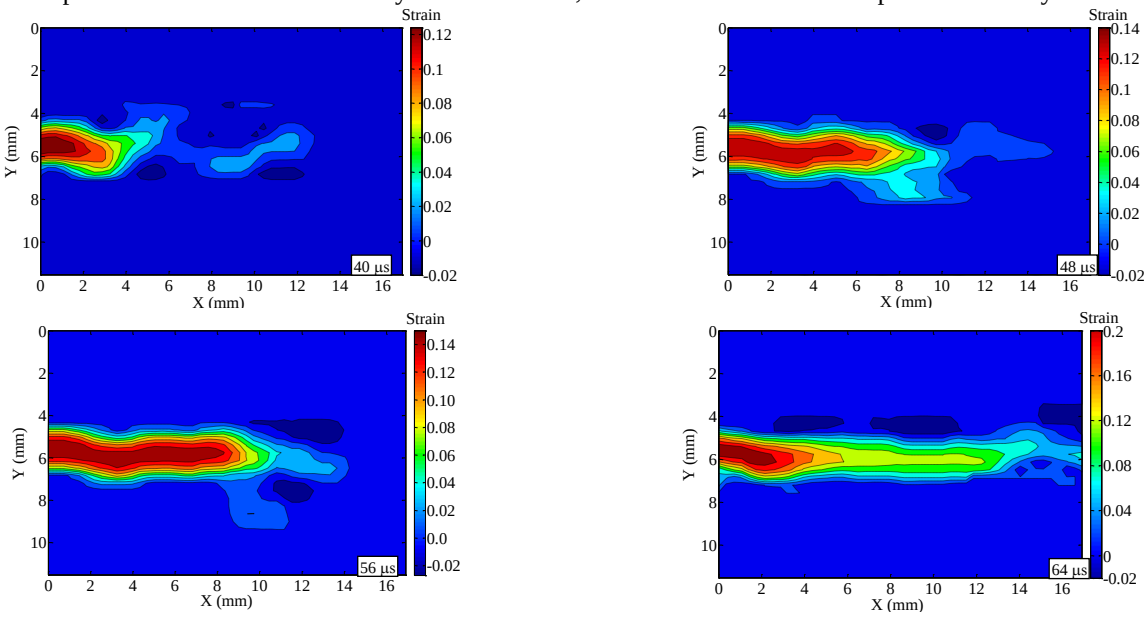

(f) Dynamic vertical strain field (unit: mm)

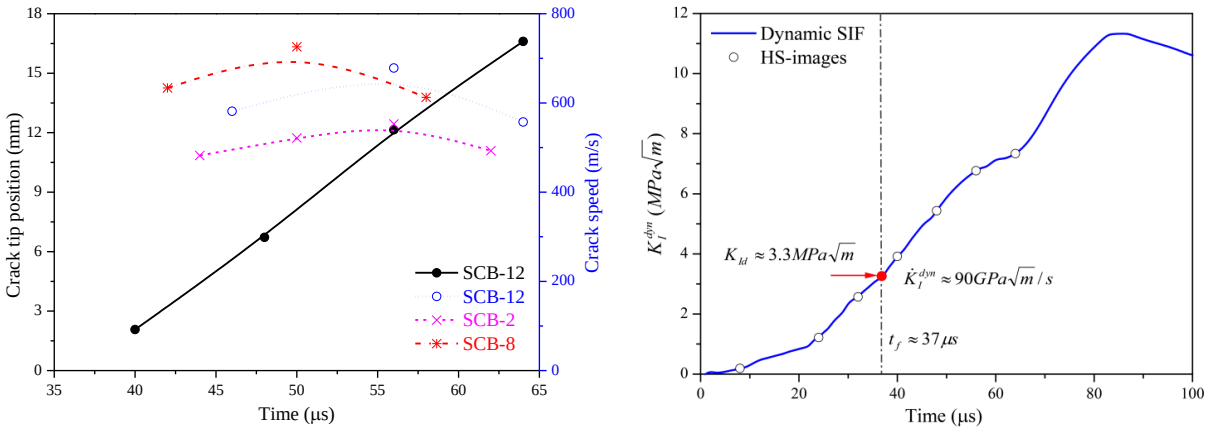

(g) Crack tip position and crack speeds (h) Evolution of dynamic SIF and the determination of K_{Id}

Fig. 5 Dynamic testing results of a typical semi-circular bending specimen

Summary

This paper proposed a detailed experimental procedure to determine Mode-I dynamic crack initiation toughness in the SHPB tests. The DIC technique combining with high-speed camera was used to measure full-field strain fields of specimens. The proposed system allows the cost-effective, non-contact, full-field strain measurements of specimens in dynamic testing methods. It is expected to become increasingly popular in the future as increasingly higher speed and higher resolution cameras and increased computing methods become more readily and economically available. A close match between strain gauges and DIC measurements has shown that the DIC technique can reliably be used to measure the surface characteristics of rock specimens under dynamic loads. And especially the DIC technique continues strain measurements after failure of the on-specimen strain gauges. It is found from the experimental results that the dynamic mechanical properties can be well determined and the high-speed DIC is a reliable full-field strain measurement method.

Acknowledgments

This work is financially supported by the Swiss National Science Foundation (No. 200020_129757) and the China Scholarship Council (CSC).

References

[1] J. Zhao, Y.X. Zhou, A.M. Hefny, J.G. Cai, S.G. Chen, H.B. Li, et al.: Tunn. Undergr. Sp. Tech. Vol. 14 (1999), P. 513-526.

[2] J.L. Shang, L.T., Shen, J. Zhao: Int. J. Rock. Mech. Min. Sci. Vol. 37 (2000), P. 705-713.

[3] J. Zhao: Int. J. Rock. Mech. Min. Sci. Vol. 37 (2000), P. 1115-1121.

[4] X.B. Li, T.S. Lok, J. Zhao: Rock. Mech. Rock. Eng. Vol. 38 (2005), P. 21-39.

[5] Y.X. Zhou, J. Zhao: Advances in rock dynamics and applications. London: CRC Press (2011).

[6] Y.X. Zhou, K. Xia, X.B. Li, H.B. Li, G.W. Ma, J. Zhao, et al.: Int. J. Rock. Mech. Min. Sci. Vol. 49 (2012), P. 105-112.

[7] P. Rastogi, E. Hack: Optical methods for solid mechanics. Berlin: Wiley-VCH (2012).

[8] W.H. Peters, W.F. Ranson: Opt. Eng. Vol. 21 (1982), P. 427-431.

[9] X.B. Li, T.S. Lok, J. Zhao, P.J. Zhao: Int. J. Rock. Mech. Min. Sci. Vol. 37 (2000), P.1055-1060.

[10] K.P. Chong, M.D. Kuruppu: Int. J. Fract. Vol. 26 (1984), P. R59-R62.

[11] I.L. Lim, I.W. Johnston, S.K. Choi: Eng. Fract. Mech. Vol. 44 (1993), P. 363-382.

[12] Q.B. Zhang, J. Zhao: submitted to Int. J. Rock. Mech. Min. Sci.